SENSITIVITY OF VIBRATION SIGNALS TO DETECT EARLY SPALLING STAGES, BY COMPARISON TO ARTIFICIAL DEFECTS INDUCED BY SPHERICAL INDENTATIONS

Adriano Gonçalves dos Passos, adriano.utfpr@gmail.com[1]
Cesar Ricardo de Oliveira, cesar.ricardo@gmail.com[1]
Cristiano Brunetti, cristiano.brunetti@renault.com[2]
Carlos Henrique da Silva, carloshs@utfpr.edu.br[1]
Giuseppe Pintaúde, pintaude@utfpr.edu.br[1]

[1]Laboratório de Superfícies e Contato (LASC) – Universidade Tecnológica Federal do Paraná (UTFPR)
[2]Renault do Brasil S.A. – Department of Materials (DEVM/DIMat-A)

Abstract. *The detection of premature failure in components subjected to rolling contact fatigue is very important and the vibration signal analysis is a powerful technique to detect the early stages of spalling. This study aims to verify the sensitivity of this methodology by comparing the results obtained evaluating the vibrational patterns in steel specimens with an artificial defect to the results obtained by measuring the signals from an austempered ductile iron (ADI). For that, it was chosen the testing model ball-on-flat. The shape of artificial defects used as a vibration standard was based on the spalling characteristics observed in ADI at previous studies and literature. Also, the smallest artificial defect produced was related to the average size of graphite nodules, a potential micro-constituent to nucleate cracks. All rolling contact fatigue tests were performed using 3.0 GPa on ADI specimens, the oil ISO 46 at 85°C was used as lubrificant mean. Piezoelectric accelerometers were used to capture the vibration signals and the signal acquired and processed in a National Instruments LabView platform (NI–LabView). The results showed that, with the current technique, there is a minimum size of artificial defect in which the signal of vibration technique is able to detect. However, this treshold showed to fully compative to the average sizes of spallings.*

Keywords: *Rolling contact fatigue; subsurface cracks; vibration signal analysis; austempered ductile iron.*

1. INTRODUCTION

Mechanical machinery under long cycles of functioning, unavoidably, suffer, at some point, from fatigue damage (Norton, 2004). However, a severe state of damaging should be avoided to ensure the safety of operators and plant (Vale, 2007). According to Almeida (2005) most of manufacturing plants that are based on the use of mechanical equipments have maintenance scheduled based on vibration signals.

Bezerra (2004) states that processing vibration signals via time-domain analysis is relative simple, on the math point of view, reliable, due large amount of samples processed, and fast, usually processed in field by dedicated devices. Root Mean Square (RMS) and Crest Factor (CF) are the most used. Moreover, Martin and Honarvar (1995) demonstrated that more complex statistical analysis provides better detection of damages, for example the fourth standardized moment commonly named Kurtosis. Many researchers have being studying vibration signals with propose of obtaining correlations with wear mechanisms with the vibration behavior of the system. Mori *et al.* (1996) managed to identify the early stages of pitting in contact fatigue tests utilizing vibration signals and wavelet transform (WTL).

Another state-of-art technique that have being used to identify several types of damages in mechanical components is the Acoustic Emission (AE), that technique used with vibration proved to be convergent and reliable to the detection of damage in rolling bearings (Passos *et al.*, 2010; Silva *et al.*, 2009; Choudhury and Tandon, 2000).

The study and detection of wear damage on materials with complex microstructure, as ADI or sinterized materials or casted components, using vibration signals is difficult. Due the high level of noise generated from the graphite nodules or even porosity the signal acquired might need be filtered. Also external factors as electric motors and mechanical couplings and components, when operating, generates extra noise to the system, that one in some scenarios being even bigger then the damage signal. Some authors as Chiementin *et al.* (2007); Mori *et al.* (1996); Purushotham *et al.* (2005) utilized advanced techniques to filter noise and isolate the signal, however those techniques usually consume heavy processing capability and time, being less viable in an industrial environment.

This paper has as main objective the development of a testing methodology to identify surface damage type spalling. Also, this work oriented to materials with homogeneous structure like steel and non-homogeneous structure like nodular irons.

2. METHODOLOGY

In the present study, to develop a methodology for identifying the damage, two sets of experiments were performed:

- Set 1: ball-on-flat tests on AISI 52100 bearing steel specimens with artificial defects.
- Set 2: ball-on-flat tests on polished Austempered Ductile Iron (ADI) specimens.

For both tests the same rig Brunetti (2008); Leite (2005); Passos *et al.* (2010) has used with few modifications like oil pump and temperature controller.

2.1 Test Rig

The tests were conducted in an equipment presented elsewhere by Brunetti *et al.* (2007) and it is composed by a horizontal chamber, in which constraint flow of heated oil controlled. Four sets of axial rolling rolling bearings are mounted and the specimen is attached to the rotational axis. Figure 1 show a partial cut of the chamber with the sample.

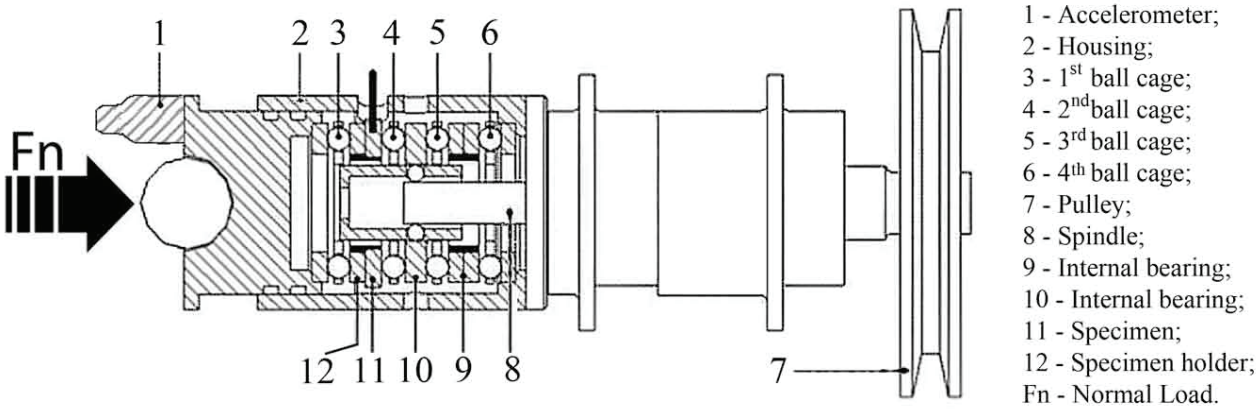

Figure 1: Sketch of contact fatigue test rig.

2.2 Vibration Signals and Acquisition

Vibration signals were captured by seismic piezoelectric accelerometer ($1025\mathrm{mV/g}$) and the signals are acquired using LabVIEW® DAQ platform. The sampling rate was 20kHz and stored in 10k sized vectors, that way the highest frequency usable had to be lower than 10kHz (Nyquist frequency) to avoid aliasing, the 10k sized vectors allowed to reconstruct buckets of 10.000 buckets of 1Hz each providing a suitable resolution without consuming too much data processing time. Figure 2 illustrates two common signals acquired on the rig. The first (a) was sampled from a non-damaged specimen, the second (b) was sampled from a single-damaged specimen and the last one (c) is a zoom-in on the grey area of the second signal.

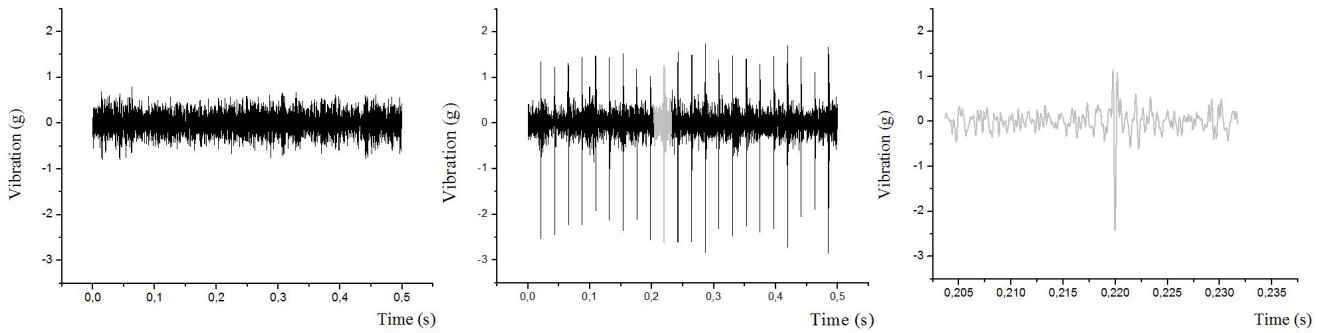

Figure 2: Examples of signals obtained after the first set of experiments.

The applied approach for signal treatment was the crest factor (FC), chosen based on previous Passos *et al.* (2010)

studies performed by the authors due to its simplicity and reliability. Equations 1 and 2 were used to calculate FC.

$$X_{\text{RMS}} = \sqrt{\frac{1}{n}\sum_{k=1}^{n} x_k^2} \tag{1}$$

$$\text{CF} = \frac{X_{\text{PEAK}}}{X_{\text{RMS}}} \tag{2}$$

2.3 Testing Conditions Overview and Hertz Theory Review

For an elastic contact between a sphere and a flat surface the contact area is a circle with radius a. Based on the bodies involved and considering an elastic contact, the radius, a, is given by the equation Eq.3. The applied load is given by W, the radius of the sphere is R and E^* is the combined Young's modulus which can be calculated with the equation Eq.4.

$$a = \left(\frac{3WR}{4E^*}\right)^{1/3} \tag{3}$$

$$\frac{1}{E^*} = \frac{1-\nu_1^2}{E_1} + \frac{1-\nu_2^2}{E^2} \tag{4}$$

For the elastic contact, a perfect rolling condition were assumed, therefore, according to Norton (2004), the static stress state equations can be used. the maximum contact pressure (P_0) at the contact area (A_c) can be defined by the equation Eq.5 and Eq.6 (Hutchings, 1992).

$$\text{P}_0 = \frac{3}{2}\left(\frac{W}{\pi a^2}\right) = \left(6\frac{WE^{*2}}{\pi^3 R^2}\right)^{1/3} \tag{5}$$

$$\text{A}_c \approx 0.83\pi\left(\frac{WR}{E^*}\right)^{2/3} \tag{6}$$

Davies (1949), based on Hertz studies, identified the location and the magnitude of the maximum shear stress (τ_{max}). The author also stated that the maximum shear stress is located at a depth equivalent to half of the contact radius, a, and its magnitude is approximately 0.31 times the maximum pressure of the contact, (P_0).

Table 1: Testing conditions overview

Material of disc	Set 1 **AISI 52100**	Set 2 **ADI**
Oil Temperature [°C]	30±1	85±2
Number of Spheres [ ]	3	3
Sphere Radius (R) [mm]	3.969	3.969
Contact Load (W) [N]	134	232
Combined Young's Modulus (E^*) [GPa]	230.8	196.72
Rockwell C Hardness (RC) [ ]	65	40
Semi-contact width (a) [mm]	0.22	0.19
Area of contact (A_c) [mm^2]	0.151	0.113
Compliance (d) [µm]	11.98	9.25
Maximum Contact Pressure (P_0) [GPa]	4	3
Maximum Shear Stress (τ_{max}) [GPa]	1.24	0.93
Shear Stress Depth ($0.5 \times a$) [µm]	110	95
Number of Specimens [ ]	6	5
Test Duration (undamaged) [cycles $\times 10^3$]	13.5	428† / 737‡
Test Duration (damaged) [cycles]	13500	225

† Earliest Failure / ‡ Latest Failure

2.3.1 Set 1, Contact Fatigue Tests on AISI 52100 Specimens With Artificial Defects

Six 51206 bearings were used as specimens, and the flat side of them were polished using 1μm alumina. These surfaces were submitted to 5 minutes run-in on the rig in order to smooth the roughness peaks. After run-in period, additional 5 minutes test were conducted to record the no-damage vibration signature (noise), and CF was calculated.

In all six specimens, spherical indentations were produced at different loads. Figure 3 shows diameter (a) and depths (b) indentations as function of the applied load.

The indented specimens were submitted 10 minutes test on the ball-on-flat rig to record the vibrational signals of each damage size.

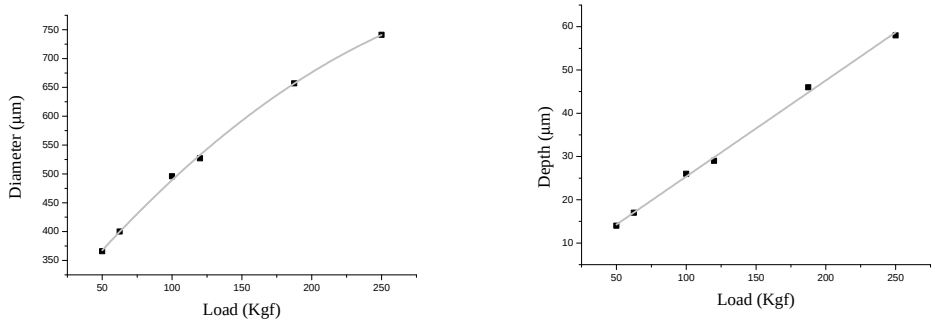

(a) (b)

Figure 3: Diameter and indentation depth as a function of applied load for spherical indentations.

2.3.2 Set 2, Contact Fatigue Tests on ADI

This second set of experiments were conducted in order to verify the ability of spalling detection using the method tested for the first set. Five specimens were produced from an ADI bar, which was turned and cut into disks of the same shape and size presented in Fig.4. After machining, the specimens were ground, sanded and polished with 1μm alumina.

The tests were performed with an active control of temperature and oil flow, maintaining the temperature at $85\pm1^{\circ}\mathrm{C}$ and the oil was delivered into the testing chamber with no pressure, keeping only a soft flow of oil in order to avoid debris accumulation.

One at each test, specimens were mounted into the pre-heated and lubricated rig's chamber. The frequency inverter were set to 1700 rpm performing a soft acceleration. When the motor achieved its full speed, the load was slowly released and the clock has started. The accelerometer constantly measured the vibration output and the computer performed the CF calculation. In order to save space and data analyzing time, only when the CF level reached 7 – or even a value higher than that – the data block was recorded in the hard drive. Also at every minute a data block was stored to track the evolution of the CF during the process. Moreover, the criteria of end-of-test was the moment that CF reached a level of more than 7 for a period of 5 seconds (10 samples).

(a) (b) (c)

Figure 4: Specimen dimensions and examples of damages on surface.

Figure 4 (a) shows an example of the FIRST set of specimens previously and after the indentation mark; (b) shows the

specimen looks; and (c) shows the surface from one of the SECOND set specimens previously and after the test.

3. RESULTS AND SICUSSIONS

At the first set of experiments, the time domain vibration signal specimens with and without artificial defects were considered for analysis, the periodic characteristic peak at the defect frequency is evident in the four deeper damage sizes as shown in Fig.5.

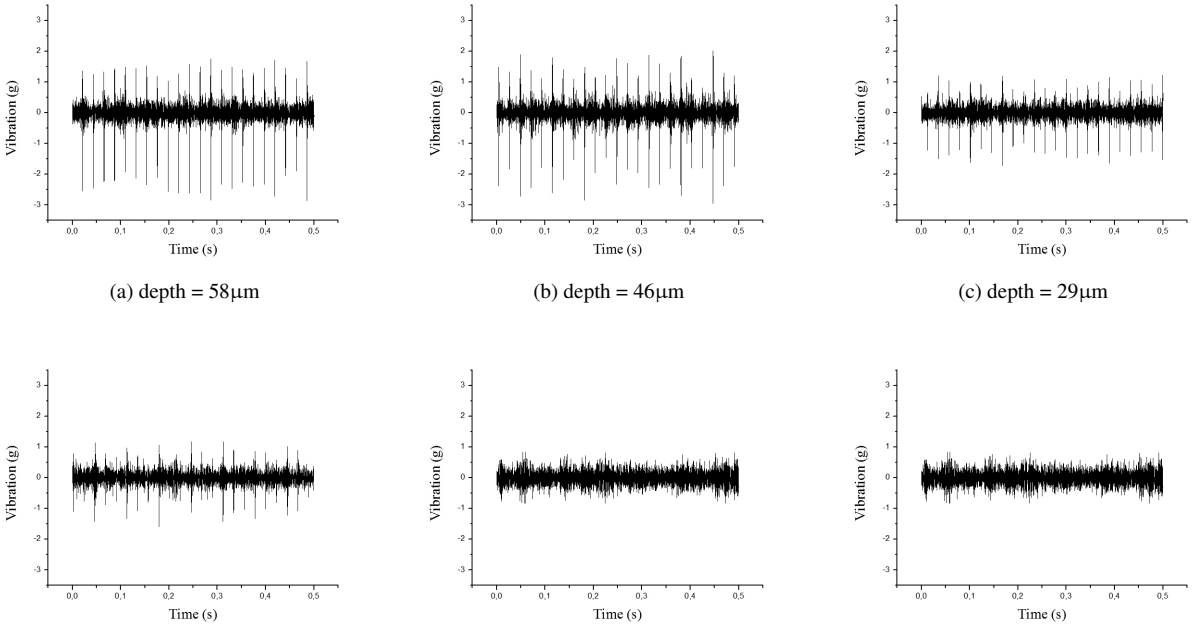

(a) depth = 58μm (b) depth = 46μm (c) depth = 29μm

(d) depth = 26μm (e) depth = 17μm (f) depth = 14μm

Figure 5: Time domain signals obtained after first set of experiments for damaged specimens.

Figure 5 show that specimens with damage below 19μm depth presented vibrational levels similar to non-damaged specimens. Therefore, this size of damage could be defined as the minimum that the equipment was capable to detect. Figure 6 presents the results of CF calculations to all 6 damaged specimens and a point that represents the undamaged states of them (0μm depth). The grey area defines the region where the technique cant detect any damage.

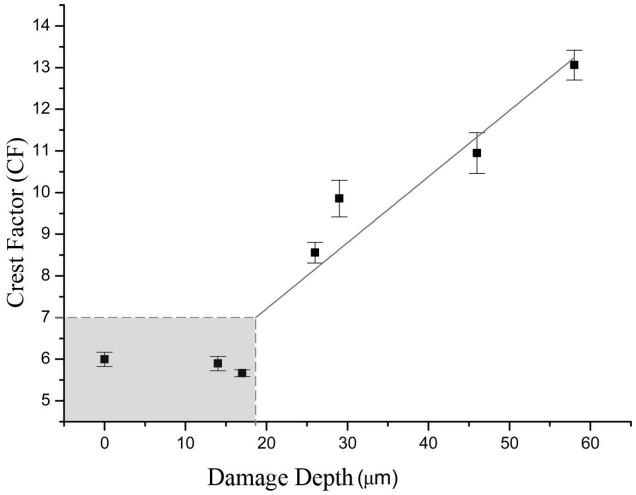

Figure 6: Crest factor as a function of damage depth (μm).

The graph also highlights the conclusion taken by the first description of the signal temporal analysis, confirming that the threshold adopted as the minimum damage size detectable by the rig, which is inferior to almost all spalling sizes presented by literature. Moreover, the definition of a CF threshold to determine the end-of-test could be considered as CF 7.

At the second set of experiments, five ADI specimens (SP) were run until the crest factor reached the value of 7 or more, which represents the early stages of a spalling. Table 2 presents the number of cycles until the failure of each specimen, as well the sizes of the spalling and the wear track near its location.

Table 2: Contact fatigue test results for ADI specimens.

SP [ ]	Load Cycles [cycles $\times 10^3$]	Spalling Size$_T$ [μm]	Spalling Size$_R$ [μm]	Wear Track [μm]
I	428	477	667	788
II	448	462	887	800
III*	563	568	802	758
IV	668	592	820	766
V**	737	585	796	788

* Non-detached / ** Partially detached
T Tangential measure / R Radial measure

A cross-section of SP II is shown in Fig.7. The bottom layer is the original micrograph taken from the specimen. On top of it, a low-opacity layer shows the theoretical shear stress distribution for the used conditions was applied. According to the Hertz contact theory, the maximum stress value at 110μm from the contact point ($0.5 \times a$). Moreover, a top layer was added with the minimum size of damage detected at the first set of experiments, to compare the size of the spalling. The first of them is the shallower, with only 20μm, and the second is significantly deeper with 100μm depth. The cut was made on the radial direction of the specimen since the isochromatics lines would not be affected by the friction.

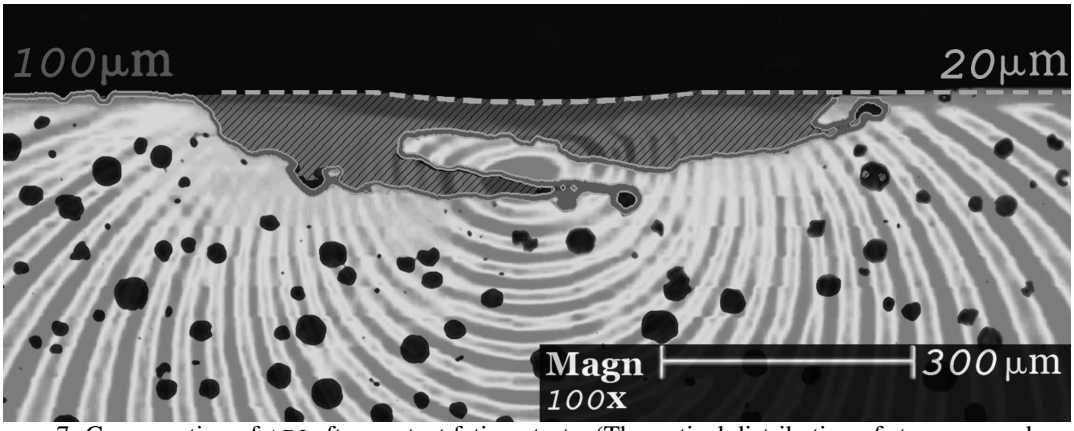

Figure 7: Cross-section of ADI after contact fatigue tests. (Theoretical distribution of stresses are shown)

Figure 7 shows the convergence between the theoretical predictions regarding the crack nucleation depth's and the spallings obtained. Also, it serves to emphasize the significantly gap between the smallest damage size that the system is capable to recognize and the real spalling size. Figure 8 shows the cross-section of SP I (a) as well the original micrograph from the radial cut of SP II (b)

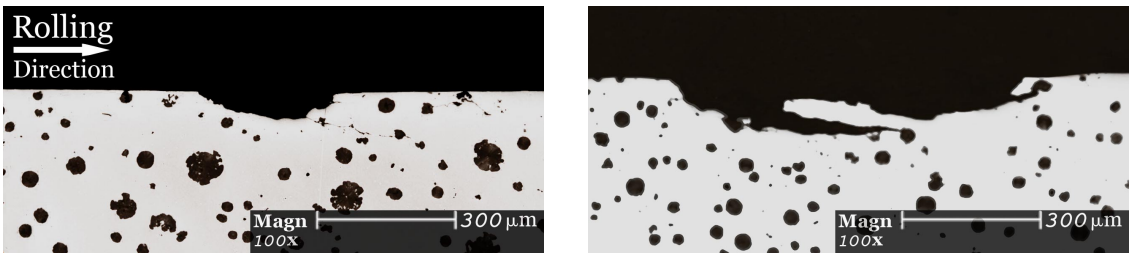

(a) (b)

Figure 8: Cross-section of ADI after contact fatigue tests.

Regarding the vibration signals, Figures 9 to 13 are divided in Fig (a) and Fig (b), in which (a) contains two graphs with CF averages and (b) contains micrograph of the respective specimen. On (a), the top graph of each figure represents the averaged CF over the test duration and the second graph magnifies the CF rising during the final 20 seconds of testing.

Crest Factor obtained from each specimen showed be compatible with the damage shape and size, allowing the authors make few assumptions regarding the development of the spalling.

Figures from 9 to 13 allowed to describe the following behaviors for each tested specimen.

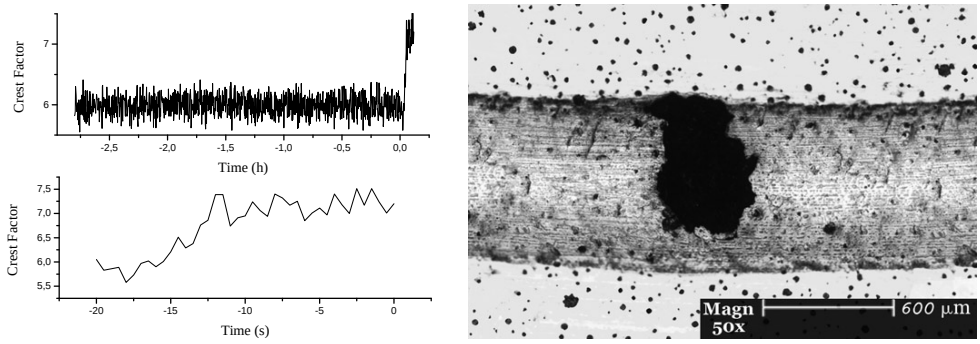

(a) (b)

Figure 9: Crest factor evolution for specimen 1 of the second set of experiments (ADI).

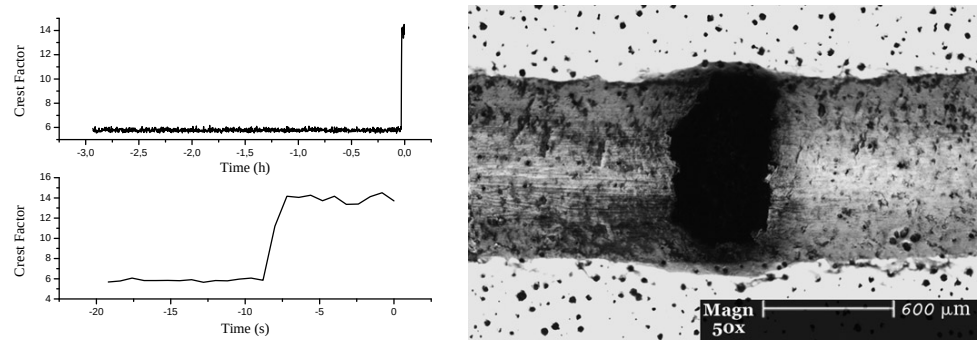

(a) (b)

Figure 10: Crest factor evolution for specimen 2 of the second set of experiments (ADI).

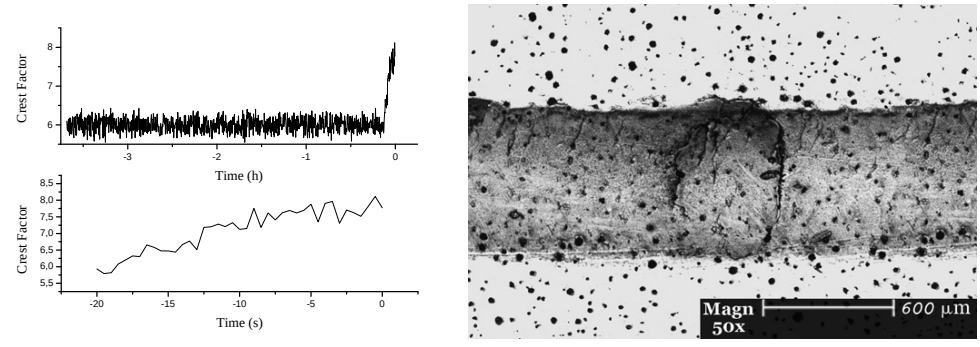

(a) (b)

Figure 11: Crest factor evolution for specimen 3 of the second set of experiments (ADI).

Specimen II and IV (Figs. 10 and 12) presented the most abrupt rising on CF, approximately from 5 to 15 in less than 200 load cycles, and both specimens presented similar large spallings suggesting the surface collapsed as a whole.

Specimen I also presented rapid rising on the CF value, but with smaller final value, approximately from 6 to 7.5 in around 250 load cycles. The lower CF value can be attributed to the non-centralized small spalling revealed on the micrograph.

On the other hand, the some careful assumptions could be done regarding SPs III and V (Figs. 11 and 13). A tooth-saw behavior is observed for the SP III, so that the CF value increased from 6 to 7.5 in more than 800 load cycles at almost stable rate. Suggesting that the size of the damage slowly increased. The corresponding micrograph revealed a non-detached spalling, suggesting also that the sub-surface cracks did not reached the surface in an enough volume to cause a detachment, but they were enough to cause instability on the area, increasing the vibration signal.

Finally, regarding SP V, the CF evolution happened in two steps. First the CF raised from 6 to 7 in approximately 300 load cycles and then abruptly raised to 8.5 in less than 50 cycles, the micrograph corroborated an idea that independent

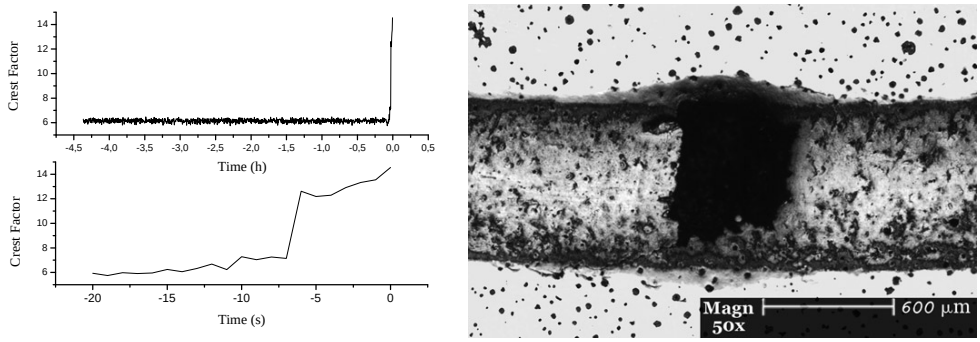

(a) (b)

Figure 12: Crest factor evolution for specimen 4 of the second set of experiments (ADI).

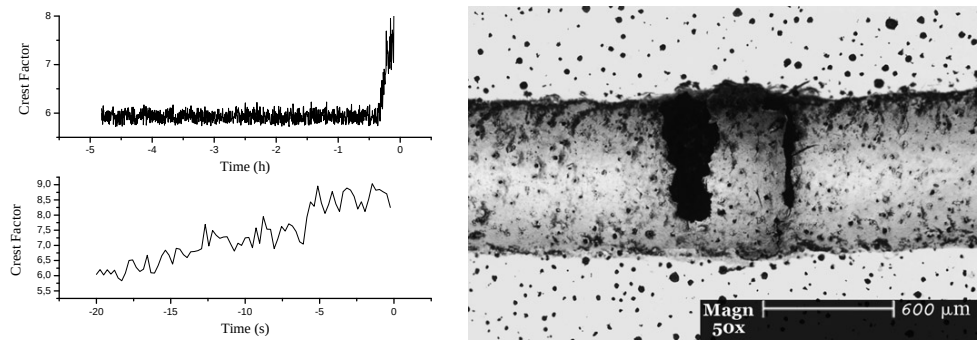

(a) (b)

Figure 13: Crest factor evolution for specimen 5 of the second set of experiments (ADI).

events occurred, there are two damages in the image and an apparent surface cracks on the edge, suggesting a near-future merge.

4. CONCLUSIONS

The first set of experiments led the authors to a solid parameter to detect verry small sizes of spalling-like damages at ball-on-flat tests. Crest Factor has also low level of mathematical complexity, allowing it to be calculated at almost real-time by a low end computer. Also the CF allowed detecting a significant band of sizes of damages, where real spallings are largely covered.

In the second set, the efficiency the method is employed to a material with complex microstructure, considering the graphite constituent of ADI, and the damage detection was satisfatory. The spalling sizes and shapes showed to be consistent with the literature.

For detection of nucleation and movements of cracks, advanced techniques, such as acustic emission, could be used.

5. ACKNOWLEDGEMENTS

The authors would like to express their sincere gratitude to the support from National Scientific and Technological Development Council CNPq (Scholarship number: 121.519/2009-0 and 135855/2010-1); Scholarship from Scientific and Technological Development Foundation of Paraná; MCT-FINEP PROMOVE 06/2006 and the companies WEG Motors S.A and Fundições Tupy Ltda.

6. REFERENCES

Almeida, M.T., 2005. "Apostila de manutenção preditiva: Confiabilidade e qualidade." <http://www.joinville.ifsc.edu.br/coral/gerenciaempresarial/> viewn at 25 Feb. 2010.

Bezerra, R.A., 2004. *Detecção de falhas em rolamentos por análise de vibração*. Ph.D. thesis, Universidade Estadual de Campinas, Campinas.

Brunetti, C., 2008. *Efeito da preparação de corpos-de-prova na vida em fadiga de contato em rolamento de ferro fundido nodular austemperado.* Master's thesis, UTFPR.

Brunetti, C., Leite, M.V. and Pintaude, G., 2007. "Effect of specimen preparation on contact fatigue wear resistance of

austempered ductile cast iron". *Wear*, Vol. 263, No. 1-6, pp. 663–668.

Chiementin, X., Bolaers, F., Cousinard, O. and Rasolofondraibe, L., 2007. "Demodulation of vibration signal using adapted Wavelet". *Journal of Bribration and Control*, Vol. 14.

Choudhury, A. and Tandon, N., 2000. "Application of acoustic emission technique for the detection of defects in rolling element bearings". *Tribology international*, Vol. 33, No. 1, pp. 39–45.

Davies, R.M., 1949. "The determination of static and dynamic yeld stresses using a steel ball". *Procedings of the Royal Society of London A*, Vol. 197, pp. 416–432.

Hutchings, I.M., 1992. *Tribology: friction and wear of engineering materials*. Ed. Butterworth, Oxford.

Leite, M.V., 2005. *Análise dos mecanismos de desgaste por fadiga de contato. Estudo de caso: ferro fundido nodular austemperado.* Master's thesis, CEFET-PR.

Martin, H.R. and Honarvar, F., 1995. "Application of statistical moments to bearing failure detection". *Applied Acousticis*, Vol. 44, pp. 67–67.

Mori, K., Kasashima, N., Yoshioka, T. and Ueno, Y., 1996. "Prediction of spalling on a ball bearing by applying the discrete wavelet transform to vibration signals". *Wear*, Vol. 195, No. 1-2, pp. 162–168.

Norton, R.L., 2004. *Projeto de máquinas: uma abordagem integrada*. Ed. Bookman, Porto alegre-RS.

Passos, A.G., Tiboni, G.B., Bronkhorst, K.B. and Silva, C.H., 2010. "Análise de sinais de vibração e emissão acústica para detecção de danos em ensaios de fadiga de contato do tipo esfera contra plano". *Congresso Nacional de Engenharia Mecânica*.

Purushotham, V., Narayanan, S. and Suryanarayana, A.N., 2005. "Multi-fault diagnosis of rolling bearing elements using wavelet analysis and hidden markov model based fault recognition". *NDTeE*.

Silva, C.H., Tiboni, G.B., Marquadt, T.A.S. and Maria, V.A.R.S., 2009. "Preliminary studies for monitoring erosion in pipelines by the acoustic emission technique". *RioPipeline conference*.

Vale, A.F.E., 2007. *Análises Estatísticas e Reconhecimento de Padrão Aplicados em Diagnósticos de Defeitos em Rolamentos Através da Análise de Vibração*. Ph.D. thesis, Universidade Federal de Itajubá.

7. Responsibility notice

The authos are the only responsible for the printed material included in this paper